

Full Length Article

Mo₂CS₂-MXene supported single-atom catalysts for efficient and selective CO₂ electrochemical reduction

Sambath Baskaran, Jaehoon Jung*

Department of Chemistry, University of Ulsan, Nam-gu, Ulsan 44776, Republic of Korea

ARTICLE INFO

Keywords:
CO₂ reduction
DFT studies
Single-atom catalysts
Heterogeneous catalysts
Electrochemical reaction

ABSTRACT

Single-atom catalysts (SACs) recently attracted considerable attention in heterogeneous catalysis, owing to high atom-utilization and unique properties. In this paper, we investigated geometry, electronic structure, stabilities, catalytic activity, and selectivity of the various TM@Mo₂CS₂ (TM = Fe, Co, Ni, Cu, Ru, Rh, Pd, Ag, Os, Ir, Pt, and Au) anchored SACs for CO₂ electrochemical reduction using periodic density functional theory and ab-initio molecular dynamics calculations. The single metal atoms tend to occupy the Mo-top site on the Mo₂CS₂ surface. Possible different reaction pathways to produce various C₁ products such as CO, HCOOH, HCHO, CH₃OH, and CH₄ have been investigated for Fe, Co, Ni, and Ru supported SACs. Among the SACs investigated, Fe, Co, and Ru supported by Mo₂CS₂ catalysts selectively produce CH₄, whereas Ru@Mo₂CS₂ has the lowest overpotential of 0.24 V. Ni primarily produces HCOOH with an overpotential is 0.37 V. Therefore, this research demonstrated the significant potential of Mo₂CS₂ surface for a single-atom catalyst for selective CO₂ reduction and other electrochemical applications.

1. Introduction

CO₂ reduction reaction (CO₂RR) by electrochemical method to produce value-added C₁ (CO, HCHO, HCOOH, CH₃OH, and CH₄) compounds beyond CO₂ capture and storage has recently gained popularity because of its potential application in sustainable energy and global warming issues [1–7]. High overpotential, poor selectivity, low faradic efficiency, and strong competition with hydrogen evolution reaction (HER) for CO₂ conversion should be resolved for achieving an efficient CO₂RR process and advancing its industrialization [8–11]. Discovering a viable CO₂RR catalyst with excellent selectivity and activity remains a difficult task.

Although transition metal (TM) heterogeneous catalysts have been widely used for CO₂RR [12–15], the single-atom catalysts (SACs) have been received considerable attention during recent years following a successful fabrication of Pt SAC implemented in FeO_x by Qiao and co-workers in 2011 [16–20]. The SACs have exceptional properties, such as high activity, selectivity, and cost efficiency, and can be used for various chemical reformations [21–41]. When compared to the traditional TM nanoparticle catalysts, the SACs can lead to maximizing the utilization of TM resources by significantly increasing the active sites that maintain their unique physicochemical properties and exceptional

catalytic activity, and thereby maximizing the cost and quantity of precious TM resources. Moreover, both experimental and theoretical studies have revealed that SACs can outperform the electrochemical CO₂RR process [42–47]. The electro reduction of CO₂ to CO and further hydrocarbon was experimentally demonstrated using Fe or Ni-doped nitrogenated carbon, of which the strong interaction with CO formed via CO₂ reduction was suggested to facilitate the protonation of CO resulting in the formation of hydrocarbon [42]. The Ni SAC was synthesized by the pyrolysis of the metal-organic framework, i.e., ZIF-8, with Ni precursor and exhibited the higher catalytic performance for selective CO₂RR compared to Ni nanoparticle with excellent current density and Faradaic efficiency [44]. A variety of single TM atoms inserted into the defect site of TiC(100) were investigated as electrochemical catalysts using computational analysis and Ir doped TiC (Ir@TiC) was proposed as an efficient SAC for CO₂RR with a low overpotential of –0.09 V [45].

A proper selection of support material is one way to improve the efficiency of SACs even further. Aside from metal and metal oxide supported SACs, two-dimensional (2D) layered materials such as hexagonal boron nitride (h-BN), TM dichalcogenides, graphdiyne, phosphorene, and graphene have piqued the interest of researchers as a support material due to their high surface area, stability, and

* Corresponding author.

E-mail address: jjung2015@ulsan.ac.kr (J. Jung).

outstanding electronic conductivity [48–58]. A class of MXene, i.e., 2D TM carbide, carbonitride, and nitride, fabricated from the MAX phase is a recent entry of the 2D layered material [59,60], and possess the specific properties, such as high stability, large specific surface area, and exceptional thermal and electrical conductivity [61,62]. The chemical properties of MXene can also be finely tuned by introducing terminal functional groups to its exterior metal atoms [63–68]. The Mo₂C MXene has recently been demonstrated to have decent electrocatalytic activity for CO₂ reduction [69–71]. The surface of MXenes, such as Ti₃C₂, Ti₂C, and Nb₂C, was experimentally reported to be terminated with halogen species and further with chalcogen species (O, S, Se, and Te) via surface exchange reactions [72], which therefore suggests the synthetic possibility of sulfur terminated Mo₂C, i.e., Mo₂CS₂ although there has yet been no experimental report on its direct synthesis. In particular, the surface-modified MXene is suitable for electrochemical processes and for anchoring TM single atoms as SACs due to the hydrophilic nature of typical terminal functional groups such as hydroxyl, oxygen, and sulfur [73–80]. As a result, MXene-based SACs are potential candidates for facilitating effective electrochemical CO₂RR catalysts.

Using periodic density functional theory (DFT) calculations, this study systematically investigates a variety of electrochemical catalytic mechanisms of CO₂RR over TM anchored on sulfur-terminated MXene (Mo₂C), i.e., Mo₂CS₂. Because the Mo₂CS₂ was computationally reported to be highly stable due to sulfur functionalization [61], it was considered as a support material for the non-noble metal SAC for CO oxidation [81]. The twelve TM elements (from d⁶ to d⁹ species) were initially screened to explore an effective SAC for CO₂RR, and thus the Fe, Co, Ni, and Ru implemented in Mo₂CS₂ were discovered to be feasible as SACs for CO₂RR by calculating the adsorption energy and by examining the competition between CO₂RR and HER. Their thermal stabilities were also explained with the ab-initio molecular dynamics (AIMD) simulation. Our computational study on the CO₂RR mechanism revealed that the C₁ compounds can be selectively based on TM species with low overpotentials (η): Ni@Mo₂CS₂ and Ru@Mo₂CS₂ SACs produce HCOOH ($\eta = 0.37$ V) and CH₄ ($\eta = 0.24$ V), respectively. As a result, we anticipate that the predicted TM@Mo₂CS₂ SACs will be promising platforms for electrochemical catalysts for selective CO₂ conversion to valuable chemicals.

2. Computation details

Spin-polarized DFT calculations were performed by the Vienna ab-initio simulation package (VASP 5.4.1) [82,83]. The interaction between core and valence electrons was described using the projector augmented wave pseudopotentials [84,85]. GGA-PBE [86,87] was used to calculate the exchange-correlation energy, with an energy cut-off of 400 eV. The 5 × 5 × 1 Monkhorst-Pack grid was used for the first Brillouin zone sampling [88]. The total energy was converged to 10⁻⁵ eV by applying the Gaussian smearing method with a width of 0.05 eV. All ions were allowed to relax until their maximum atomic forces fell below 0.02 eV/Å. To account for van der Waals (vdW) interactions, Grimme's DFT-D3 method [89] was used. In the periodically repeated slab model, a vacuum layer of 20 Å was used to remove interlayer interaction. The 2D monolayer Mo₂CS₂ was built by a 4 × 4 supercell comprising 16 C, 32 S, and 32 Mo atoms. AIMD simulations with the NVT ensemble technique were performed at 500 K using a Nose-Hoover thermostat [90,91] for 10 ps with a time step of 2.0 fs to investigate the thermal stability of SACs. A grid-based Bader population analysis [92] was used to compute the charge redistribution.

The binding energy of the TM atom on the Mo₂CS₂ is defined as.

$$\Delta E_b = E_{\text{TM}@\text{Mo}_2\text{CS}_2} - E_{\text{Mo}_2\text{CS}_2} - E_{\text{TM}} \quad (1)$$

where $E_{\text{TM}@\text{Mo}_2\text{CS}_2}$ is the total energy of TM implemented Mo₂CS₂, i.e., TM@Mo₂CS₂; $E_{\text{Mo}_2\text{CS}_2}$ is the energy of the clean Mo₂CS₂; E_{TM} is the energy of the single TM atom. The adsorption energy of the intermediate

species during the catalytic reaction was calculated from.

$$\Delta E_{\text{ads}} = E_{\text{total}} - E_{\text{TM}@\text{Mo}_2\text{CS}_2} - E_{\text{adsorbate}} \quad (2)$$

where E_{total} , $E_{\text{TM}@\text{Mo}_2\text{CS}_2}$, and $E_{\text{adsorbate}}$ are corresponding to the energies for TM@Mo₂CS₂ with adsorbed species, TM@Mo₂CS₂, and free adsorbates, respectively. The computational hydrogen electrode model was used to calculate the Gibbs free energy of each fundamental step [93]:

$$\Delta G = \Delta E + \Delta ZPE - T\Delta S + \Delta G_U + \Delta G_{\text{pH}} \quad (3)$$

where ΔE is the electronic energy differences directly obtained from DFT calculations; ΔZPE is the change of the zero-point energy; ΔS is the change in the entropy at the temperature T. ΔG_U is the applied electrode potential and ΔG_{pH} is the effect of pH on Gibbs free energy, with the pH of the acidic condition assumed to be zero. Particularly, the zero-point energies and entropies of intermediate species during the electrochemical CO₂RR process were calculated by using their vibrational frequencies, and the Gibbs free energy corrections to gas-phase molecules were obtained from the NIST database (<https://cccbdb.nist.gov>). The overpotential (η) and limiting potential (U_L) are important parameters for estimating the performance of the catalysts. The U_L was calculated using the following equation:

$$U_L = -\Delta G/e \quad (4)$$

where $-\Delta G$ is the change of Gibbs free energy for the rate-limiting step. The η for electrochemical CO₂RR process was calculated by.

$$\eta = U_{\text{eq}} - U_L \quad (5)$$

where U_{eq} is the equilibrium potential (-0.250 V for HCOOH and 0.169 V for CH₄) [94–96].

3. Results and discussion

3.1. Adsorption of single transition metal atoms on Mo₂CS₂ monolayer

The 2D monolayer of sulfur-terminated Mo₂C, i.e., Mo₂CS₂ is made up of five atomic layers (Fig. 1): the innermost C atoms are located at the octahedral site of Mo atoms that are terminated with the outermost S atoms, and thus all Mo atoms are coordinated with three C and three S

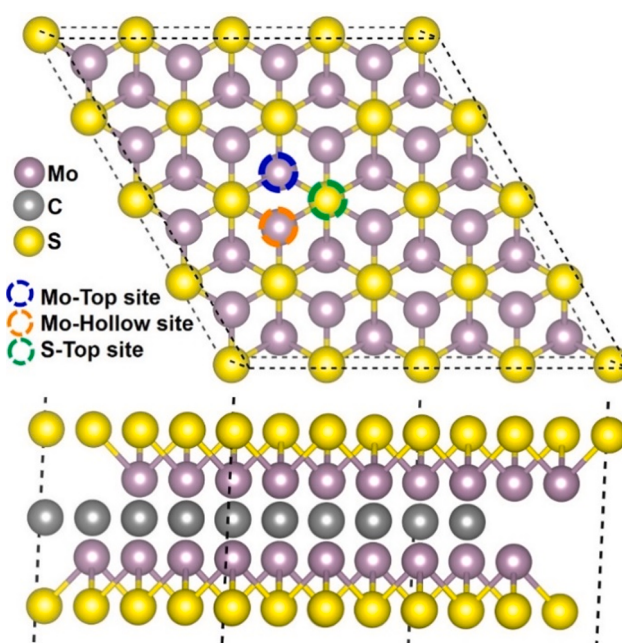


Fig. 1. Top and side views of optimized 4 × 4 Mo₂CS₂ supercell.

atoms. The optimized lattice constant of Mo_2CS_2 is $a = b = 3.08 \text{ \AA}$ and the interatomic distances are 2.20 and 2.04 \AA for Mo-C and Mo-S, respectively, as reported previously [61]. There are three different sites available for the adsorption of TM atoms on Mo_2CS_2 , i.e., Mo-top, Mo-hollow, and S-top sites as depicted in Fig. 1 (see also Fig. S1). The twelve TM elements (from d^6 to d^9 species; Fe, Co, Ni, and Cu for 3d TM; Ru, Rh, Pd, and Ag for 4d TM; Os, Ir, Pt, and Au for 5d TM) were initially screened to investigate an effective SAC for CO_2RR . The individual TM atoms, except Ag and Au, desire to occupy the Mo-top site on the Mo_2CS_2 surface compared to other adsorption sites. Whereas the binding energies (ΔE_b) of Ag and Au are less than -1.5 eV , the majority of the TM atoms have considerable ΔE_b values of more than -2.5 eV (Fig. 2). As a result of their low ΔE_b in comparison to other TM species, Ag and Au were not considered for further calculations. The TM atoms are directly coordinated with the three adjacent sulfur atoms with the TM-S bond distances, $d_{\text{TM-S}}$, ranging from 1.93 to 2.11 \AA , except Ag and Au ($d_{\text{Ag-S}} = d_{\text{Au-S}} = 2.60 \text{ \AA}$) (see Table S1).

3.2. Screening TM@ Mo_2CS_2 SACs: CO_2RR vs. HER

The electrochemical CO_2RR process is highly competing with HER reaction, and thus suppressing HER is a critical issue in developing the efficient electrochemical CO_2RR catalysts [11]. Therefore, to determine the feasibility of TM@ Mo_2CS_2 SACs for electrochemical CO_2RR process, we studied the three different adsorption intermediates, ${}^*\text{H}$, ${}^*\text{COOH}$, and ${}^*\text{OCHO}$ on TM@ Mo_2CS_2 (* denotes the active site of SAC), because these are key intermediates to determining the selectivity of catalytic reaction. We primarily quantitatively compared the Gibbs free energies (ΔG) for the formation of ${}^*\text{COOH}$ and ${}^*\text{OCHO}$ intermediates that are formed via the first protonation of CO_2 (${}^* + \text{CO}_2 + \text{H}^+ + \text{e}^- \rightarrow {}^*\text{COOH}$ or ${}^*\text{OCHO}$) as well as the formation of ${}^*\text{H}$ (${}^* + \text{H}^+ + \text{e}^- \rightarrow \text{H}^*$) as a key intermediate of HER on TM@ Mo_2CS_2 (Fig. 3). The higher negative ΔG corresponds to the more favorable formation of intermediate species on TM@ Mo_2CS_2 . The dashed line indicates $\Delta G({}^*\text{COOH} \text{ or } {}^*\text{OCHO}) = \Delta G({}^*\text{H})$, and therefore the SACs above and below the dashed line indicate are HER selective and CO_2RR selective, respectively. The comparative study revealed that Fe, Co, Ni, Cu, and Ru SACs are CO_2RR selective when compared to HER, with Ni, Cu, and Ru preferentially forming ${}^*\text{OCHO}$, and Fe and Co SACs forming both (${}^*\text{COOH}$ and ${}^*\text{OCHO}$) intermediates. Overall the electrochemical CO_2RR processes could be achieved with the 3d TM SACs compared to the 4d and 5d TM species except Ru.

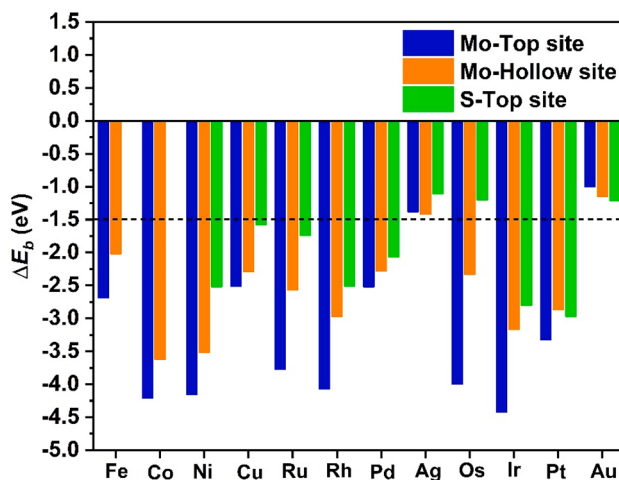


Fig. 2. Calculated binding energy (ΔE_b) of single TM atoms on the $4 \times 4 \text{ Mo}_2\text{CS}_2$ supercell. The binding energies of TM atom at S-top site for Fe@ Mo_2CS_2 and Co@ Mo_2CS_2 are not presented as they are highly unstable and will transform to Mo-hollow site.

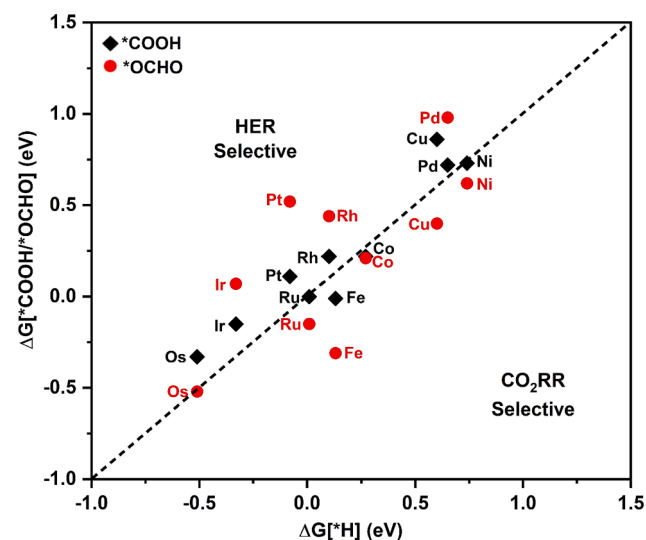


Fig. 3. Comparative plot of Gibbs free energy (ΔG) for the first protonation step in the CO_2RR and the hydrogen evolution reaction on TM@ Mo_2CS_2 . The dashed line indicates $\Delta G({}^*\text{COOH} \text{ or } {}^*\text{OCHO}) = \Delta G({}^*\text{H})$, and thus SACs below the dotted line are CO_2RR selective.

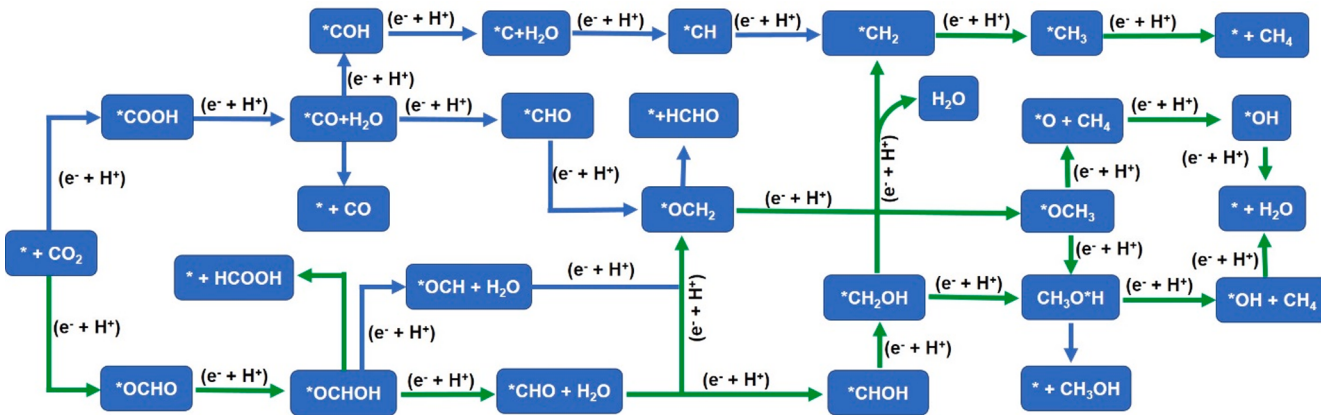
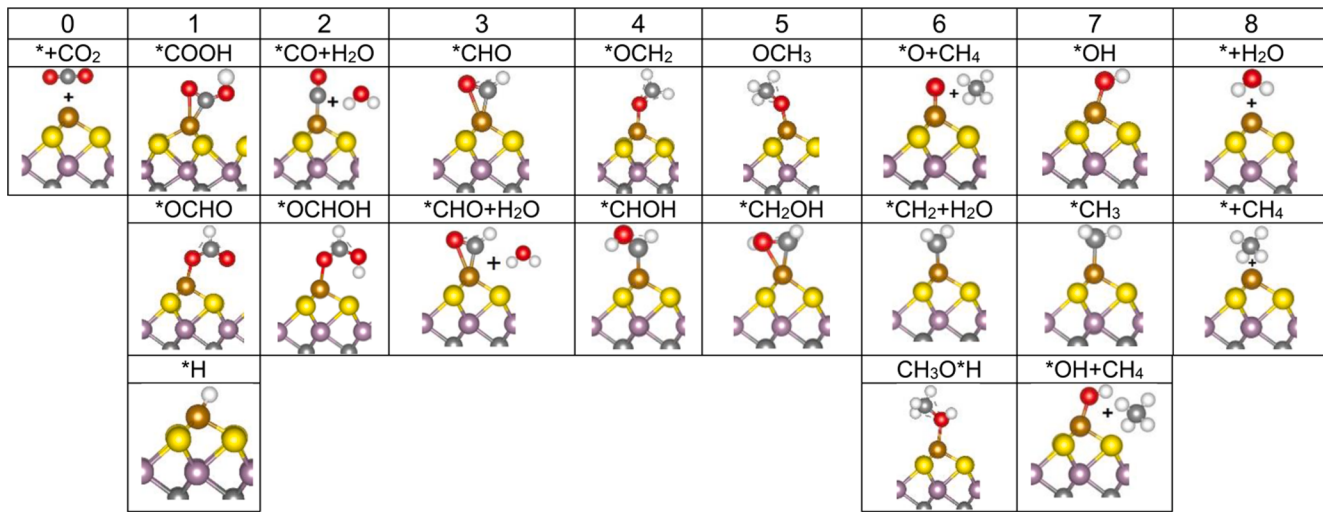
3.3. Thermal stability and electronic structure of TM@ Mo_2CS_2

The optimized TM-S bond distances, $d_{\text{TM-S}}$ (TM = Fe, Co, Ni, Cu, Ru), are shorter than the sum of single bond covalent radii except for Cu@ Mo_2CS_2 (see Table S1), indicating the strong covalent metal-support interaction (CMSI) [97]. Furthermore, the AIMD simulations were conducted to determine the thermal stability of SACs at high temperatures. During the AIMD simulation of 10 ps at 500 K, the diffusion of TM atom on Mo_2CS_2 and the significant structural fluctuation in TM-S bond distances were not observed except for Cu@ Mo_2CS_2 (see Figs. S2 and S3). One of the major causes of catalytic performance degradation is the aggregation of individual TM atoms during repeated catalytic cycles. As a result, we ran the AIMD simulation (10 ps, 500 K) with two TM atoms (TM = Fe, Co, Ni, and Ru) on Mo_2CS_2 of the identical 4×4 supercell (see Fig. S4). During AIMD simulation with two TM atoms, individual TM atoms maintained their adsorption position, i.e., Mo-top site, and thus the proposed SACs would be considered highly stable enough for preventing the formation of TM clusters on Mo_2CS_2 .

To better understand the strong interaction between TM and Mo_2CS_2 based on their electronic structures, we examined the Bader charge, electron density difference (EDD) maps, and projected density of state (PDOS) of TM@ Mo_2CS_2 (TM = Fe, Co, Ni, and Ru). The fact that all of the TM atoms have a positive atomic charge indicates that charge transfer occurs from the TM atom to Mo_2CS_2 (see Table S1), confirming that strong interaction between TM atoms and Mo_2CS_2 . The EDD maps also agree with the electron redistribution caused by charge transfer (Fig. S5). The strong overlap between the TM d orbitals and the S 3p orbitals of Mo_2CS_2 was discovered for all the TM SACs, corresponding to the strong electronic coupling through the hybridization between them around the Fermi level.

3.4. Reaction mechanisms of electrochemical CO_2RR on TM@ Mo_2CS_2

The detailed mechanistic reaction pathways for electrochemical CO_2RR were investigated using TM@ Mo_2CS_2 SACs (TM = Fe, Co, Ni, and Ru) that were selected by systematically examining the structural and thermal stabilities and the electronic structures. Scheme 1 and Fig. 4 show the possible pathways to various types of C₁ products, as well as the geometric structures of key reaction intermediates in the electrochemical CO_2RR process. DFT calculations were used to determine the lowest energy pathways for electrochemical CO_2RR on TM SACs (Fig. 5).

Scheme 1. Possible reaction pathways for the electrochemical CO₂RR on TM@Mo₂CS₂.Fig. 4. Important reaction intermediates in electrochemical CO₂RR process on TM@Mo₂CS₂.

The first step in the electro reduction of CO₂ may involve hydrogenation, which involves binding with a proton and gaining one electron, resulting in the formation of two distinct intermediates, *OCHO and *COOH, according to the binding position of a proton. While the formation of *COOH and *OCHO intermediates compete for the Co SAC, the Fe, Ru, and Ni SACs primarily lead to the formation of the *OCHO intermediate. The second hydrogenation following the formation of intermediates, *COOH and *OCHO, can produce the 2e⁻ C₁ products, carbon monoxide (CO) and formic acid (HCOOH), through the reaction pathways, *COOH + H⁺ + e⁻ → *CO + H₂O → * + CO and *OCHO + H⁺ + e⁻ → *OCHOH → * + HCOOH, respectively. However, the calculated ΔG values required for the desorption of CO on TM@Mo₂CS₂ are greater than 1 eV for all the SACs, indicating that CO production is not viable (Table S2). The production of HCOOH is significantly more favored with the rate-limiting ΔG of less than 0.80 eV for its desorption on all the studied SACs when compared to CO production. In particular, the Ni SAC has the lowest ΔG value of 0.43 eV for the desorption of HCOOH, which is lower than those of Fe (0.76), Co (0.56), and Ru (0.56 eV) SACs.

Further hydrogenation of *CO and *OCHOH instead of the desorption from the SAC surface may result in the formation of three distinct intermediates, *CHO, *COH, and *OCH (Scheme 1). As displayed in Fig. 5, the ΔG required to form *CHO intermediate is significantly lower than that required to form *COH and *OCH intermediates. Therefore, the pathway involving the formation of *CHO is an energetically feasible route for the electrochemical CO₂RR on TM@Mo₂CS₂, except Ni SAC.

The formation of *CHO is also caused by *OCHOH intermediate for all the SACs considered in this study (Fig. 5): the pathway *OCHO + H⁺ + e⁻ → *OCHOH followed by *OCHOH + H⁺ + e⁻ → *CHO + H₂O is more energetically favorable than the pathway *COOH + H⁺ + e⁻ → *CO + H₂O followed by *CO + H⁺ + e⁻ → *CHO. However, the desorption as HCOOH from *OCHOH is easier than the formation of *CHO by 0.60 eV only on Ni@Mo₂CS₂ (Fig. 5d), and thus Ni SAC is expected to selectively produce HCOOH among a variety of C₁ compounds producible via CO₂RR. The HCOOH formation is unfavorable to *CHO formation by 0.09, 0.11, and -0.06 eV for Fe, Co, and Ru SACs, respectively (Fig. 5a-c).

The continuous hydrogenation of intermediate *CHO can result in the formation of formaldehyde (HCHO), methanol (CH₃OH), and methane (CH₄) as displayed in Scheme 1. The desorption energies of formaldehyde, methanol, and methane on TM@Mo₂CS₂ (TM = Fe, Co, and Ru) presented in Table S2 indicate that the formation of CH₄ is only the major product of their electrochemical CO₂RR processes with the negative desorption energies: -0.38, -0.98, and -0.83 eV for Fe, Co, and Ru SACs, respectively. Furthermore, we discovered that the most energetically favorable pathway for CO₂RR on TM@Mo₂CS₂ (TM = Fe, Co, and Ru) is toward the formation of CH₄. The Fe, Co, and Ru SACs proceed through the pathways *OCH₃ + H⁺ + e⁻ → *O + CH₄ (Fig. 5a), CH₃O*H + H⁺ + e⁻ → *OH + CH₄ (Fig. 5b), and *CH₂OH + H⁺ + e⁻ → *CH₂ + H₂O followed by *CH₂ + H⁺ + e⁻ → *CH₃ and further *CH₃ + H⁺ + e⁻ → CH₄ (Fig. 5c), respectively.

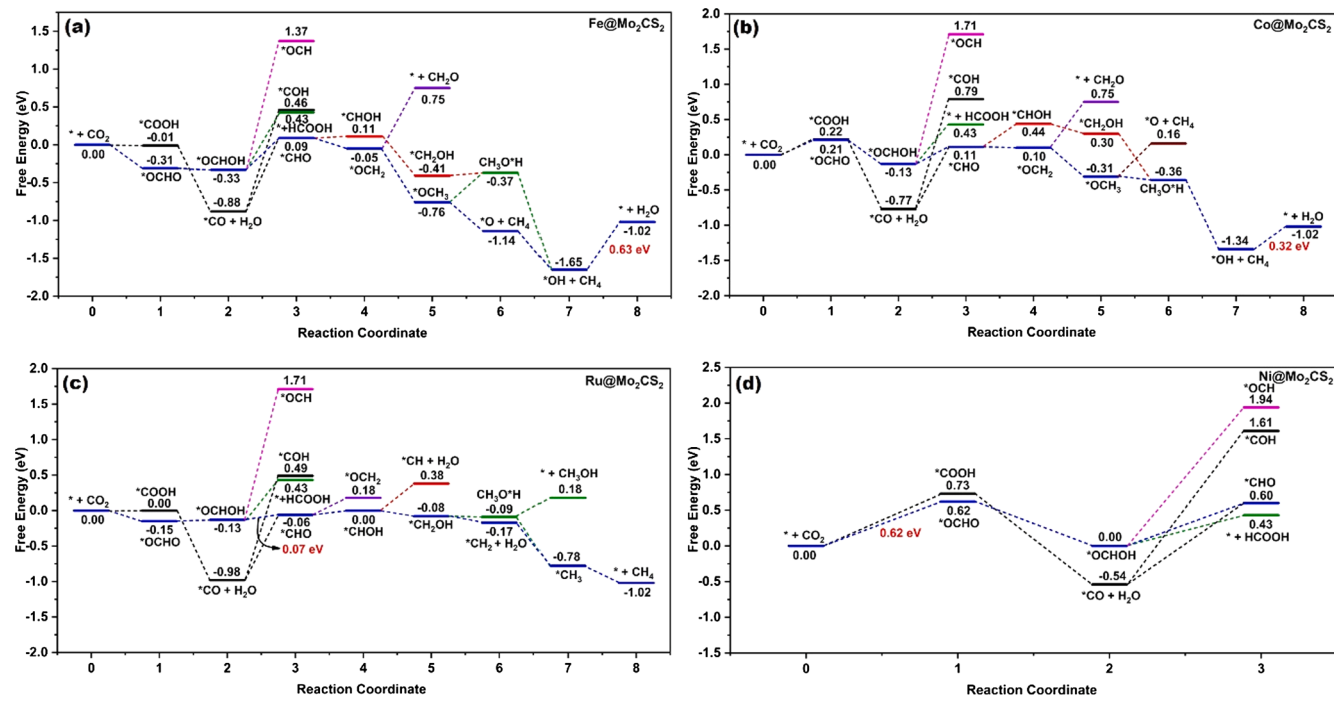


Fig. 5. Computed Gibbs free energy (ΔG) diagrams of the electrochemical CO₂RR on TM@Mo₂CS₂ (TM = (a) Fe, (b) Co, (c) Ru, and (d) Ni) at zero potential.

Path (1): *COH \rightarrow *C + H₂O \rightarrow *CH \rightarrow *CH₂ \rightarrow *CH₃ \rightarrow * + CH₄
 Path (2): *CHO \rightarrow *OCH₂ \rightarrow *OCH₃ \rightarrow O* + CH₄ \rightarrow *OH \rightarrow * + H₂O
 Path (3): *CHO \rightarrow *OCH₂ \rightarrow *OCH₃ \rightarrow H*OCH₃ \rightarrow *OH + CH₄ \rightarrow * + H₂O
 Path (4): *CHO \rightarrow *CHOH \rightarrow *CH₂OH \rightarrow *CH₂ + H₂O \rightarrow *CH₃ \rightarrow * + CH₄

It is well understood that the lower the free energy barrier of reaction, the energetically easier the chemical conversion. For the reaction paths for producing CH₄, we excluded path (1) because of the high instability of the intermediate *COH for TM@Mo₂CS₂ (TM = Fe, Co, and Ru) as previously mentioned. (Note that each arrow involves one proton and one electron in paths (1)-(4) in which H₂O or CH₄ molecule produced during the overall reaction does not take part in next reaction.) By comparing the calculated free energy barriers of the remaining three reaction paths (2, 3, and 4), we discovered that the Fe, Co, and Ru SACs go through the CO₂RR process to produce CH₄ via the reaction path (2), (3), and (4), respectively.

The overpotential is the vital parameter in determining the performance of SACs in the experimental application. As the overpotential becomes decreases, the energy requirement, i.e., externally applied potential, for chemical conversion can be reduced further. Hence, the SACs for CO₂RR must have a lower overpotential used as a potential catalyst. The potential determining steps (PDS), limiting potentials (U_L), equilibrium potential (U_{eq}) of different reduction products, and overpotentials (η) for CO₂RR process on TM@Mo₂CS₂ (TM = Fe, Co, Ru, and Ni) are presented in Table 1. The strong hybridization between TM d orbital and O 2p orbital of the potential determining intermediates

(*OH for Fe and Co SACs; *OCHOH for Ru SAC; *OCHO for Ni SAC), which was confirmed by PDOS analysis (see Fig. S6), indicates that a significant amount of energy is required to proceed to the next reaction step. The PDS of Fe and Co SACs is *OH + H⁺ + e⁻ \rightarrow * + H₂O, and their η values are 0.80 and 0.49 V, respectively. Although the CO₂RR product of Ru SAC, i.e., CH₄, is identical to those of Fe and Co SACs, the reaction energy profile of Ru SAC is significantly different from that of Fe and Co SACs. The PDS for Ru SAC is *OCHOH + H⁺ + e⁻ \rightarrow *CHO + H₂O with η = 0.24 V, which is much lower than the values for Fe and Co SACs. In particular, the η value of Ru@Mo₂CS₂ SAC is much lower compared to that previously reported for heterogenous copper catalyst (Cu(211), η = 0.77 V) [15], and thus indicates its high potential as an electrochemical CO₂RR catalyst. The Ni SAC leading to the different reduction product, i.e., HCOOH, has the PDS of * + CO₂ + H⁺ + e⁻ \rightarrow *OCHO and a relatively low value of η = 0.37 V. Additionally, to evaluate the catalytic efficiency of TM@Mo₂CS₂ SACs obtained by employing the terminal sulfur groups and by introducing the isolated TM atoms as a catalytic active species, we also investigated the CO₂RR processes on pristine Mo₂C MXene of which the catalytic active site is surface Mo atoms (see Figs. S7 and S8). The first stable intermediate species is *OCHO formed through the pathway * + CO₂ + H⁺ + e⁻ \rightarrow *OCHO with ΔG of -1.39 eV and then the CH₄ is suggested as the most favorable product through further hydrogenation steps. The formation of first intermediate species *OCHO on Mo₂C is highly exothermic compared to those on TM@Mo₂CS₂ SACs (see Fig. 5). However, the reaction energy (1.07 eV) of PDS, i.e., *OH + H⁺ + e⁻ \rightarrow * + H₂O, is highly endothermic and thus results in the η value of 1.24 V which is much larger than the corresponding values for TM@Mo₂CS₂ SACs. Therefore, our computational results show that TM@Mo₂CS₂ SACs can provide excellent catalytic performance for the electrochemical CO₂RR process while maintaining a low overpotential and high selectivity.

Furthermore, to understand the influence of solvent medium, i.e., aqueous environment (dielectric constant of water, ϵ = 78.54) [98], on the free energy profile for CO₂RR on TM@Mo₂CS₂ (TM = Fe, Co, Ru, and Ni), we used implicit self-consistent solvent model using VASPsol [99,100] software (Fig. S9) in a manner of single-point calculation. The major C₁ products determined in gas-phase calculations were retained for all TM@Mo₂CS₂ SACs although the different PDS of each reaction

Table 1

Potential determining steps (PDS), limiting potentials (U_L), equilibrium potential (U_{eq}) of different reduction products, and overpotentials (η) for the CO₂RR process on TM@Mo₂CS₂ (TM = Fe, Co, Ru, and Ni).

Systems (product)	PDS	U _L (V)	U _{eq} (V)	η (V)
Fe@Mo ₂ CS ₂ (CH ₄)	*OH + H ⁺ + e ⁻ \rightarrow * + H ₂ O	-0.63	0.169	0.80
Co@Mo ₂ CS ₂ (CH ₄)	*OH + H ⁺ + e ⁻ \rightarrow * + H ₂ O	-0.32	0.169	0.49
Ru@Mo ₂ CS ₂ (CH ₄)	*OCHOH + H ⁺ + e ⁻ \rightarrow *CHO + H ₂ O	-0.07	0.169	0.24
Ni@Mo ₂ CS ₂ (HCOOH)	* + CO ₂ + H ⁺ + e ⁻ \rightarrow *OCHO	-0.62	-0.250	0.37

(except for Ru@Mo₂CS₂ SAC) was obtained. The PDS for Fe@Mo₂CS₂ is *OCHOH + H⁺ + e⁻ → *CHO + H₂O ($\Delta G_{\text{sol}} = 0.27$ eV) (Fig. S9a), with the ΔG value is significantly lower than $\Delta G_{\text{gas}} = 0.63$ eV for the PDS, *OH + H⁺ + e⁻ → * + H₂O, determined by gas-phase calculation. For Co@Mo₂CS₂ SAC, the *COOH is more stable than the *OCHO, and thus the reaction mechanism and PDS being shifted from *OH + H⁺ + e⁻ → * + H₂O ($\Delta G_{\text{gas}} = 0.32$ eV) to *CO + H⁺ + e⁻ → *CHO ($\Delta G_{\text{sol}} = 0.77$ eV) (Fig. S9b). For Ru@Mo₂CS₂ SAC, the formation of *COOH and *OCHO intermediates are highly competitive (Fig. S9c), and the CO₂RR process toward CH₄ via *OCHO was discovered to be energetically more feasible. Similarly, Ni@Mo₂CS₂ SAC also has a highly competitive formation of *COOH and *OCHO intermediates (Fig. S9d) that are highly stabilized due to solvent effect, and thus the PDS is shifted from the formation of *OCHO ($\Delta G_{\text{gas}} = 0.62$ eV) to the formation of HCOOH ($\Delta G_{\text{sol}} = 0.18$ eV). The ΔG_{sol} values for the PDS of Fe@Mo₂CS₂ and Ni@Mo₂CS₂ are considerably reduced compared to the corresponding values obtained from the gas-phase calculation by 0.36 and 0.54 eV, respectively. Therefore, our DFT calculations with applied implicit self-consistent solvent model imply that Fe@Mo₂CS₂ and Ni@Mo₂CS₂ could be efficient for electrochemical CO₂RR catalysis to produce CH₄ and HCOOH, respectively.

4. Conclusions

In conclusion, we performed periodic DFT calculations to investigate the geometry, catalytic activity, and selectivity of various Mo₂CS₂ (MXene) anchored SACs for electrochemical CO₂ reduction, of which the stabilities were also examined with AIMD simulation. The adsorption energy indicates that the single transition metal atoms tend to occupy the Mo-top site on the Mo₂CS₂ surface. Considering the competition against HER, TM@Mo₂CS₂ (TM = Fe, Co, Ni, and Ru) SACs show good selectivity for CO₂ reduction. While Fe, Co, and Ru SACs selectively produce CH₄ with overpotentials of 0.80, 0.49, and 0.24 V, respectively, the Ni SAC primarily produces HCOOH with an overpotential of 0.37 V. Therefore, we anticipate that the predicted TM@Mo₂CS₂ SACs will have promising catalytic activity toward CO₂ reduction. Our computational insights can provide strong impetus for utilizing various MXene materials as a support of SACs.

CRediT authorship contribution statement

Sambath Baskaran: Conceptualization, Formal analysis, Investigation, Writing – original draft. **Jaehoon Jung:** Conceptualization, Writing – review & editing, Supervision.

Declaration of Competing Interest

The authors declare that they have no known competing financial interests or personal relationships that could have appeared to influence the work reported in this paper.

Acknowledgements

This work was supported by the next-generation carbon upcycling project (2020M1A2A6079679) through the National Research Foundation funded by the Ministry of Science and ICT, Republic of Korea.

Appendix A. Supplementary material

Supplementary data to this article can be found online at <https://doi.org/10.1016/j.apsusc.2022.153339>.

References

- [1] M. North, P. Styring, Faraday Discuss. 183 (2015) 489–502, <https://doi.org/10.1039/C5FD90077H>.
- [2] D.D. Zhu, J.L. Liu, S.Z. Qiao, Adv. Mater. 28 (2016) 3423–3452, <https://doi.org/10.1002/adma.201504766>.
- [3] C. Song, Catal. Today 115 (2006) 2–32, <https://doi.org/10.1016/j.cattod.2006.02.029>.
- [4] E.A. Quadrelli, G. Centi, J.-L. Duplan, S. Perathoner, ChemSusChem 4 (2011) 1194–1215, <https://doi.org/10.1002/cssc.201100473>.
- [5] D.U. Nielsen, X.-M. Hu, K. Daasbjerg, T. Skrydstrup, Nat. Catal. 1 (2018) 244–254, <https://doi.org/10.1038/s41929-018-0051-3>.
- [6] X. Lu, D. Jin, S. Wei, Z. Wang, C. An, W. Guo, J. Mater. Chem. A 3 (2015) 12118–12132, <https://doi.org/10.1039/C4TA06829G>.
- [7] D. Gao, R.M. Arán-Ais, H.S. Jeon, B. Roldan Cuena, Nat. Catal. 2 (2019) 198–210, <https://doi.org/10.1038/s41929-019-0235-5>.
- [8] C.H. Lee, M.W. Kanan, ACS Catal. 5 (2015) 465–469, <https://doi.org/10.1021/cs501767z>.
- [9] Y. Hori, H. Wakebe, T. Tsukamoto, O. Koga, Electrochim. Acta 39 (1994) 1833–1839, [https://doi.org/10.1016/0013-4686\(94\)85172-7](https://doi.org/10.1016/0013-4686(94)85172-7).
- [10] C. Dong, J. Fu, H. Liu, T. Ling, J. Yang, S.Z. Qiao, X.-W. Du, J. Mater. Chem. A 5 (2017) 7184–7190, <https://doi.org/10.1039/C6TA10733H>.
- [11] S. Nitopi, E. Bertheussen, S.B. Scott, X. Liu, A.K. Engstfeld, S. Horch, B. Seger, I.E. L. Stephens, K. Chan, C. Hahn, J.K. Nørskov, T.F. Jaramillo, I. Chorkendorff, Chem. Rev. 119 (2019) 7610–7672, <https://doi.org/10.1021/acs.chemrev.8b00705>.
- [12] X. Nie, M.R. Esopi, M.J. Janik, A. Asthagiri, Angew. Chem. Int. Ed. 52 (2013) 2459–2462, <https://doi.org/10.1002/anie.201208320>.
- [13] C. Liu, T.R. Cundari, A.K. Wilson, J. Phys. Chem. C 116 (2012) 5681–5688, <https://doi.org/10.1021/jp210480c>.
- [14] K.P. Kuhl, T. Hatsukade, E.R. Cave, D.N. Abram, J. Kibsgaard, T.F. Jaramillo, J. Am. Chem. Soc. 136 (2014) 14107–14113, <https://doi.org/10.1021/ja505791r>.
- [15] C. Shi, K. Chan, J.S. Yoo, J.K. Nørskov, Org. Process Res. Dev. 20 (2016) 1424–1430, <https://doi.org/10.1021/acs.oprd.6b00103>.
- [16] B. Qiao, A. Wang, X. Yang, L.F. Allard, Z. Jiang, Y. Cui, J. Liu, J. Li, T. Zhang, Nat. Chem. 3 (2011) 634–641, <https://doi.org/10.1038/nchem.1095>.
- [17] X.-F. Yang, A. Wang, B. Qiao, J. Li, J. Liu, T. Zhang, Acc. Chem. Res. 46 (2013) 1740–1748, <https://doi.org/10.1021/ar300361m>.
- [18] J. Liu, ACS Catal. 7 (2017) 34–59, <https://doi.org/10.1021/acscatal.6b01534>.
- [19] L. Liu, A. Corma, Chem. Rev. 118 (2018) 4981–5079, <https://doi.org/10.1021/acs.chemrev.7b00776>.
- [20] J. Liu, B.R. Bunes, L. Zang, C. Wang, Environ. Chem. Lett. 16 (2018) 477–505, <https://doi.org/10.1007/s10311-017-0679-2>.
- [21] Z. Chen, J. Zhao, C.R. Cabrera, Z. Chen, Small Methods 3 (2019) 1800368, <https://doi.org/10.1002/smtd.201800368>.
- [22] Y. Feng, Q. Wan, H. Xiong, S. Zhou, X. Chen, X.I. Pereira Hernandez, Y. Wang, S. Lin, A.K. Datye, H. Guo, J. Phys. Chem. C 122 (2018) 22460–22468, <https://doi.org/10.1021/acs.jpcc.8b05815>.
- [23] J. Jones, H. Xiong, A.T. DeLaRiva, E.J. Peterson, H. Pham, S.R. Challa, G. Qi, S. Oh, M.H. Wiebenga, X.I. Pereira Hernández, Y. Wang, A.K. Datye, Science 353 (2016) 150, <https://doi.org/10.1126/science.aaf8800>.
- [24] F. Li, L. Li, X. Liu, X.C. Zeng, Z. Chen, ChemPhysChem 17 (2016) 3170–3175, <https://doi.org/10.1002/cphc.201600540>.
- [25] F. Li, Y. Li, X.C. Zeng, Z. Chen, ACS Catal. 5 (2015) 544–552, <https://doi.org/10.1021/cs501790v>.
- [26] X. Li, W. Bi, L. Zhang, S. Tao, W. Chu, Q. Zhang, Y. Luo, C. Wu, Y. Xie, Adv. Mater. 28 (2016) 2427–2431, <https://doi.org/10.1002/adma.201505281>.
- [27] C. Ling, L. Shi, Y. Ouyang, X.C. Zeng, J. Wang, Nano Lett. 17 (2017) 5133–5139, <https://doi.org/10.1021/acs.nanolett.7b02518>.
- [28] J.M. Thomas, Nature 525 (2015) 325–326, <https://doi.org/10.1038/525325a>.
- [29] A. Wang, J. Li, T. Zhang, Nat. Rev. Chem. 2 (2018) 65–81, <https://doi.org/10.1038/s41570-018-0010-1>.
- [30] Z. Wang, J. Zhao, J. Wang, C.R. Cabrera, Z. Chen, J. Mater. Chem. A 6 (2018) 7547–7556, <https://doi.org/10.1039/C8TA00875B>.
- [31] H. Zhang, G. Liu, L. Shi, J. Ye, Adv. Energy Mater. 8 (2018) 1701343, <https://doi.org/10.1002/aenm.201701343>.
- [32] L. Zhang, Y. Ren, W. Liu, A. Wang, T. Zhang, Natl. Sci. Rev. 5 (2018) 653–672, <https://doi.org/10.1093/nsr/nwy077>.
- [33] S. Baskaran, C.-Q. Xu, Y.-F. Jiang, Y.-G. Wang, J. Li, ChemPhysChem 22 (2021) 378–385, <https://doi.org/10.1002/cphc.202000950>.
- [34] X. Li, Y. Zeng, C.-W. Tung, Y.-R. Lu, S. Baskaran, S.-F. Hung, S. Wang, C.-Q. Xu, J. Wang, T.-S. Chan, H.M. Chen, J. Jiang, Q. Yu, Y. Huang, J. Li, T. Zhang, B. Liu, ACS Catal. 11 (2021) 7292–7301, <https://doi.org/10.1021/acscatal.1c01621>.
- [35] S.H. Talib, S. Hussain, S. Baskaran, Z. Lu, J. Li, ACS Catal. 10 (2020) 11951–11961, <https://doi.org/10.1021/acscatal.0c01175>.
- [36] S.H. Talib, X. Yu, Q. Yu, S. Baskaran, J. Li, Sci. China Mater. 63 (2020) 1003–1014, <https://doi.org/10.1007/s04843-020-1399-y>.
- [37] Z. Zhang, C. Feng, C. Liu, M. Zuo, L. Qin, X. Yan, Y. Xing, H. Li, R. Si, S. Zhou, J. Zeng, Nat. Commun. 11 (2020) 1215, <https://doi.org/10.1038/s41467-020-14917-6>.
- [38] L. Wang, C. Zhu, M. Xu, C. Zhao, J. Gu, L. Cao, X. Zhang, Z. Sun, S. Wei, W. Zhou, W.-X. Li, J. Lu, J. Am. Chem. Soc. 143 (2021) 18854–18858, <https://doi.org/10.1021/jacs.1c09498>.
- [39] K. Gu, F. Wei, Y. Cai, S. Lin, H. Guo, J. Phys. Chem. Lett. 12 (2021) 8423–8429, <https://doi.org/10.1021/acs.jpclett.1c02019>.
- [40] L. Gao, F. Wang, M.-A. Yu, F. Wei, J. Qi, S. Lin, D. Xie, J. Mater. Chem. A 7 (2019) 19838–19845, <https://doi.org/10.1039/C9TA06470B>.
- [41] J. Li, L. Sun, Q. Wan, J. Lin, S. Lin, X. Wang, J. Phys. Chem. Lett. 12 (2021) 11415–11421, <https://doi.org/10.1021/acs.jpclett.1c02762>.

- [42] A.S. Varela, N. Ranjbar Sahraie, J. Steinberg, W. Ju, H.-S. Oh, P. Strasser, Angew. Chem. Int. Ed. 54 (2015) 10758–10762, <https://doi.org/10.1002anie.201502099>.
- [43] K. Mori, T. Taga, H. Yamashita, ACS Catal. 7 (2017) 3147–3151, <https://doi.org/10.1021/acscatal.7b00312>.
- [44] C. Zhao, X. Dai, T. Yao, W. Chen, X. Wang, J. Wang, J. Yang, S. Wei, Y. Wu, Y. Li, J. Am. Chem. Soc. 139 (2017) 8078–8081, <https://doi.org/10.1021/jacs.7b02736>.
- [45] S. Back, Y. Jung, ACS Energy Lett. 2 (2017) 969–975, <https://doi.org/10.1021/acsenergylett.7b00152>.
- [46] S. Back, J. Lim, N.-Y. Kim, Y.-H. Kim, Y. Jung, Chem. Sci. 8 (2017) 1090–1096, <https://doi.org/10.1039/C6SC03911A>.
- [47] X. Wang, Z. Chen, X. Zhao, T. Yao, W. Chen, R. You, C. Zhao, G. Wu, J. Wang, W. Huang, J. Yang, X. Hong, S. Wei, Y. Wu, Y. Li, Angew. Chem. Int. Ed. 57 (2018) 1944–1948, <https://doi.org/10.1002anie.201712451>.
- [48] H. Liu, A.T. Neal, Z. Zhu, Z. Luo, X. Xu, D. Tománek, P.D. Ye, ACS Nano 8 (2014) 4033–4041, <https://doi.org/10.1021/nn501226z>.
- [49] L. Li, Y. Yu, G.J. Ye, Q. Ge, X. Ou, H. Wu, D. Feng, X.H. Chen, Y. Zhang, Nat. Nanotechnol. 9 (2014) 372–377, <https://doi.org/10.1038/nano.2014.35>.
- [50] G. Li, Y. Li, H. Liu, Y. Guo, Y. Li, D. Zhu, Chem. Commun. 46 (2010) 3256–3258, <https://doi.org/10.1039/B92273D>.
- [51] X. Gao, H. Liu, D. Wang, J. Zhang, Chem. Soc. Rev. 48 (2019) 908–936, <https://doi.org/10.1039/C8CS00773J>.
- [52] T. Wang, K. Andrews, A. Bowman, T. Hong, M. Koehler, J. Yan, D. Mandrus, Z. Zhou, Y.-Q. Xu, Nano Lett. 18 (2018) 2766–2771, <https://doi.org/10.1021/acs.nanolett.7b04205>.
- [53] A. Allain, A. Kis, ACS Nano 8 (2014) 7180–7185, <https://doi.org/10.1021/nn5021538>.
- [54] W. Yuan, G. Shi, J. Mater. Chem. A 1 (2013) 10078–10091, <https://doi.org/10.1039/C3TA11774J>.
- [55] B. Radisavljevic, A. Radenovic, J. Brivio, V. Giacometti, A. Kis, Nat. Nanotechnol. 6 (2011) 147–150, <https://doi.org/10.1038/nano.2010.279>.
- [56] K.S. Novoselov, V.I. Fal'ko, L. Colombo, P.R. Gellert, M.G. Schwab, K. Kim, Nature 490 (2012) 192–200, <https://doi.org/10.1038/nature11458>.
- [57] C. Huang, C. Li, G. Shi, Energy Environ. Sci. 5 (2012) 8848–8868, <https://doi.org/10.1039/C2EE22238H>.
- [58] A.K. Geim, Science 324 (2009) 1530–1534, <https://doi.org/10.1126/science.1158877>.
- [59] M. Naguib, O. Mashtalir, J. Carle, V. Presser, J. Lu, L. Hultman, Y. Gogotsi, M. W. Barsoum, ACS Nano 6 (2012) 1322–1331, <https://doi.org/10.1021/nn204153h>.
- [60] M. Naguib, M. Kurtoglu, V. Presser, J. Lu, J. Niu, M. Heon, L. Hultman, Y. Gogotsi, M.W. Barsoum, Adv. Mater. 23 (2011) 4248–4253, <https://doi.org/10.1002/adma.201102306>.
- [61] M. Khazaei, M. Arai, T. Sasaki, M. Estili, Y. Sakka, Phys. Chem. Chem. Phys. 16 (2014) 7841–7849, <https://doi.org/10.1039/C4CP00467A>.
- [62] J.-C. Lei, X. Zhang, Z. Zhou, Front. Phys. 10 (2015) 276–286, <https://doi.org/10.1007/s11467-015-0493-x>.
- [63] A.D. Handoko, K.H. Kho, T.L. Tan, H. Jin, Z.W. Seh, J. Mater. Chem. A 6 (2018) 21885–21890, <https://doi.org/10.1039/C8TA06567E>.
- [64] H. Chen, A.D. Handoko, J. Xiao, X. Feng, Y. Fan, T. Wang, D. Legut, Z.W. Seh, Q. Zhang, A.C.S. Appl. Mater. Interfaces 11 (2019) 36571–36579, <https://doi.org/10.1021/acsami.9b00941>.
- [65] H. Chen, A.D. Handoko, T. Wang, J. Qu, J. Xiao, X. Liu, D. Legut, Z. Wei Seh, Q. Zhang, ChemSusChem 13 (2020) 5690–5698, <https://doi.org/10.1002/cssc.202001624>.
- [66] J. Peng, X. Chen, W.-J. Ong, X. Zhao, N. Li, Chem 5 (2019) 18–50, <https://doi.org/10.1016/j.chempr.2018.08.037>.
- [67] A.D. Handoko, S.N. Steinmann, Z.W. Seh, Nanoscale Horiz. 4 (2019) 809–827, <https://doi.org/10.1039/C9NH00100J>.
- [68] N. Li, J. Peng, W.-J. Ong, T. Ma, Arramel, P. Zhang, J. Jiang, X. Yuan, C. Zhang, Matter 4 (2021) 377–407, <https://doi.org/10.1016/j.matt.2020.10.024>.
- [69] Z. Guo, Y. Li, B. Sa, Y. Fang, J. Lin, Y. Huang, C. Tang, J. Zhou, N. Miao, Z. Sun, Appl. Surf. Sci. 521 (2020), 146436, <https://doi.org/10.1016/j.apsusc.2020.146436>.
- [70] N. Li, X. Chen, W.-J. Ong, D.R. MacFarlane, X. Zhao, A.K. Cheetham, C. Sun, ACS Nano 11 (2017) 10825–10833, <https://doi.org/10.1021/acsnano.7b03738>.
- [71] K.R.G. Lim, A.D. Handoko, S.K. Nemani, B. Wyatt, H.-Y. Jiang, J. Tang, B. Anasori, Z.W. Seh, ACS Nano 14 (2020) 10834–10864, <https://doi.org/10.1021/acsnano.0c05482>.
- [72] V. Kamysbayev, A.S. Filatov, H. Hu, X. Rui, F. Lagunas, D. Wang, R.F. Klie, D. V. Talapin, Science 369 (2020) 979–983, <https://doi.org/10.1126/science.aba8311>.
- [73] S. Wang, L. Li, K. San Hui, F. Bin, W. Zhou, X. Fan, E. Zalnezhad, J. Li, K.N. Hui, Adv. Eng. Mater. 23 (2021) 2100405, <https://doi.org/10.1002/adem.202100405>.
- [74] Z. Chen, S. Huang, B. Huang, M. Wan, N. Zhou, Appl. Surf. Sci. 509 (2020), 145319, <https://doi.org/10.1016/j.apsusc.2020.145319>.
- [75] D. Zhao, Z. Chen, W. Yang, S. Liu, X. Zhang, Y. Yu, W.-C. Cheong, L. Zheng, F. Ren, G. Ying, X. Cao, D. Wang, Q. Peng, G. Wang, C. Chen, J. Am. Chem. Soc. 141 (2019) 4086–4093, <https://doi.org/10.1021/jacs.8b13579>.
- [76] J. Zhang, Y. Zhao, X. Guo, C. Chen, C.-L. Dong, R.-S. Liu, C.-P. Han, Y. Li, Y. Gogotsi, G. Wang, Nat. Catal. 1 (2018) 985–992, <https://doi.org/10.1038/s41929-018-0195-1>.
- [77] C. Cheng, X. Zhang, M. Wang, S. Wang, Z. Yang, Phys. Chem. Chem. Phys. 20 (2018) 3504–3513, <https://doi.org/10.1039/C7CP07161B>.
- [78] Y. Zhang, R. Zhan, Q. Xu, H. Liu, M. Tao, Y. Luo, S. Bao, C. Li, M. Xu, Chem. Eng. J. 357 (2019) 220–225, <https://doi.org/10.1016/j.cej.2018.09.142>.
- [79] Z. Fan, Y. Wang, Z. Xie, D. Wang, Y. Yuan, H. Kang, B. Su, Z. Cheng, Y. Liu, Adv. Sci. 5 (2018) 1800750, <https://doi.org/10.1002/advs.201800750>.
- [80] Z. Guo, J. Zhou, L. Zhu, Z. Sun, J. Mater. Chem. A 4 (2016) 11446–11452, <https://doi.org/10.1039/C6TA04414J>.
- [81] S.H. Talib, S. Baskaran, X. Yu, Q. Yu, B. Bashir, S. Muhammad, S. Hussain, X. Chen, J. Li, Sci. China Mater. 64 (2021) 651–663, <https://doi.org/10.1007/s40843-020-1458-5>.
- [82] G. Kresse, J. Furthmüller, Comput. Mater. Sci. 6 (1996) 15–50, [https://doi.org/10.1016/0927-0256\(96\)00008-0](https://doi.org/10.1016/0927-0256(96)00008-0).
- [83] G. Kresse, J. Furthmüller, Phys. Rev. B: Condens. Matter Mater. Phys. 54 (1996) 11169–11186, <https://doi.org/10.1103/PhysRevB.54.11169>.
- [84] P.E. Blöchl, Phys. Rev. B: Condens. Matter Mater. Phys. 50 (1994) 17953–17979, <https://doi.org/10.1103/PhysRevB.50.17953>.
- [85] G. Kresse, D. Joubert, Phys. Rev. B: Condens. Matter Mater. Phys. 59 (1999) 1758–1775, <https://doi.org/10.1103/PhysRevB.59.1758>.
- [86] J.P. Perdew, J.A. Chevary, S.H. Vosko, K.A. Jackson, M.R. Pederson, D.J. Singh, C. Fiolhais, Phys. Rev. B: Condens. Matter Mater. Phys. 46 (1992) 6671–6687, <https://doi.org/10.1103/PhysRevB.46.6671>.
- [87] J.P. Perdew, K. Burke, M. Ernzerhof, Phys. Rev. Lett. 77 (1996) 3865–3868, <https://doi.org/10.1103/PhysRevLett.77.3865>.
- [88] H.J. Monkhorst, J.D. Pack, Phys. Rev. B: Condens. Matter Mater. Phys. 13 (1976) 5188–5192, <https://doi.org/10.1103/PhysRevB.13.5188>.
- [89] S. Grimme, J. Antony, S. Ehrlich, H. Krieg, J. Chem. Phys. 132 (2010) 154104–154119, <https://doi.org/10.1063/1.3382344>.
- [90] S. Nosé, J. Chem. Phys. 81 (1984) 511–519, <https://doi.org/10.1063/1.447334>.
- [91] W.G. Hoover, Phys. Rev. A 31 (1985) 1695–1697, <https://doi.org/10.1103/PhysRevA.31.1695>.
- [92] G. Henkelman, A. Arnaldsson, H. Jónsson, Comput. Mater. Sci. 36 (2006) 354–360, <https://doi.org/10.1016/j.commatsci.2005.04.010>.
- [93] J.K. Nørskov, J. Rossmeisl, A. Logadottir, L. Lindqvist, J.R. Kitchin, T. Bligaard, H. Jónsson, J. Phys. Chem. B 108 (2004) 17886–17892, <https://doi.org/10.1021/jp047349j>.
- [94] Z. Gu, H. Shen, L. Shang, X. Lv, L. Qian, G. Zheng, Small Methods 2 (2018) 1800121, <https://doi.org/10.1002/smtd.201800121>.
- [95] S. Garg, M. Li, A.Z. Weber, L. Ge, L. Li, V. Rudolph, G. Wang, T.E. Rufford, J. Mater. Chem. A 8 (2020) 1511–1544, <https://doi.org/10.1039/C9TA13298H>.
- [96] J. Qiao, Y. Liu, F. Hong, J. Zhang, Chem. Soc. Rev. 43 (2014) 631–675, <https://doi.org/10.1039/C3CS60323G>.
- [97] B. Qiao, J.-X. Liang, A. Wang, C.-Q. Xu, J. Li, T. Zhang, J.J. Liu, Nano Res. 8 (2015) 2913–2924, <https://doi.org/10.1007/s12274-015-0796-9>.
- [98] J. Rossmeisl, A. Logadottir, J.K. Nørskov, Chem. Phys. 319 (2005) 178–184, <https://doi.org/10.1016/j.chemphys.2005.05.038>.
- [99] K. Mathew, R. Sundararaman, K. Letchworth-Weaver, T.A. Arias, R.G. Hennig, J. Chem. Phys. 140 (2014), 084106, <https://doi.org/10.1063/1.4865107>.
- [100] K. Mathew, V.S.C. Kolluru, S. Mula, S.N. Steinmann, R.G. Hennig, J. Chem. Phys. 151 (2019), 234101, <https://doi.org/10.1063/1.5132354>.